High levels of cyclic diguanylate interfere with beneficial bacterial colonization

Ruth Y. Isenberg[1,2], David G. Christensen[3], Karen L. Visick[3], and Mark J. Mandel[1,2,*]

[1] Department of Medical Microbiology and Immunology, University of Wisconsin-Madison, Madison, WI USA

[2] Microbiology Doctoral Training Program, University of Wisconsin-Madison, Madison, WI USA

[3] Department of Microbiology and Immunology, Loyola University Stritch School of Medicine, Chicago, IL USA

Short title: c-di-GMP during *V. fischeri* colonization

Keywords: *Vibrio fischeri*, microbiome, *Euprymna scolopes*, squid, c-di-GMP, biofilm, flagellar motility

* Correspondence to:

Mark J. Mandel
University of Wisconsin-Madison
Department of Medical Microbiology and Immunology
1550 Linden Drive
Madison, WI 53706
Phone: (608) 261-1170
Fax: (608) 262-8418
Email: mmandel@wisc.edu

ABSTRACT

During colonization of the Hawaiian bobtail squid (*Euprymna scolopes*), *Vibrio fischeri* bacteria undergo a lifestyle transition from a planktonic motile state in the environment to a biofilm state in host mucus. Cyclic diguanylate (c-di-GMP) is a cytoplasmic signaling molecule that is important for regulating motility-biofilm transitions in many bacterial species. *V. fischeri* encodes 50 proteins predicted to synthesize and/or degrade c-di-GMP, but a role for c-di-GMP regulation during host colonization has not been investigated. We examined strains exhibiting either low or high levels of c-di-GMP during squid colonization and found that while a low c-di-GMP strain had no colonization defect, a high c-di-GMP strain was severely impaired. Expression of a heterologous c-di-GMP phosphodiesterase restored colonization, demonstrating that the effect is due to high c-di-GMP levels. In the constitutive high c-di-GMP state, colonizing *V. fischeri* exhibited reduced motility, altered biofilm aggregate morphology, and a transcriptional regulatory interaction between two key polysaccharides, cellulose and Syp. Our results highlight the importance of proper c-di-GMP regulation during beneficial animal colonization, illustrate multiple pathways regulated by c-di-GMP in the host, and uncover an interplay of multiple exopolysaccharide systems in host-associated aggregates.

IMPORTANCE

There is substantial interest in studying cyclic diguanylate (c-di-GMP) in pathogenic and environmental bacteria, which has led to an accepted paradigm in which high c-di-GMP levels promote biofilm formation and reduce motility. However, considerably less focus has been placed on understanding how this compound contributes to beneficial colonization. Using the *Vibrio fischeri*-Hawaiian bobtail squid study system, we took advantage of recent genetic advances in the bacterium to modulate c-di-GMP levels and measure colonization and track c-di-GMP phenotypes in a symbiotic interaction. Studies in the animal host revealed a c-di-GMP-

dependent interaction between two distinct biofilm polysaccharides, Syp and cellulose, that was not evident in culture-based studies: elevated c-di-GMP altered the composition and abundance of the *in vivo* biofilm by decreasing Syp transcription due to increased cellulose synthesis. This study reveals important parallels between pathogenic and beneficial colonization and additionally identifies c-di-GMP-dependent regulation that occurs specifically in the squid host.

INTRODUCTION

In both pathogenic and beneficial associations, bacteria transition from a motile, planktonic state in the environment to a surface-associated biofilm state within the host. Cyclic diguanylate (c-di-GMP) is an intracellular signaling molecule that regulates this lifestyle transition for many bacterial species, including *Vibrio cholerae*, *Pseudomonas aeruginosa*, *Caulobacter crescentus*, and *Agrobacterium tumefaciens* (Heindl et al., 2014; Hengge et al., 2016). Generally, higher intracellular c-di-GMP concentrations lead to increased biofilm formation and decreased motility, while lower intracellular c-di-GMP concentrations lead to the opposite phenotypes. C-di-GMP levels are regulated by diguanylate cyclase (DGC) proteins, which synthesize c-di-GMP, and phosphodiesterase (PDE) proteins, which degrade c-di-GMP. DGCs contain a GGDEF domain and PDEs contain either an EAL or HD-GYP domain. While the effects of c-di-GMP on motility, biofilm formation, and infectivity of pathogens such as *V. cholerae* have been extensively studied (Römling et al., 2013), the impact of c-di-GMP during the establishment of beneficial bacterial symbioses is not well understood. The focus of this study is to examine how c-di-GMP impacts beneficial colonization in a system where we can manipulate intracellular levels of the compound and dissect the colonization process in detail.

85 *Vibrio fischeri* is the exclusive, beneficial light organ symbiont of the Hawaiian bobtail squid
86 (*Euprymna scolopes*). *V. fischeri* undergoes the motility-to-biofilm lifestyle transition during the
87 initiation of host colonization (Ludvik et al., 2021; Nyholm et al., 2000; Visick, 2009; Yip et al.,
88 2006). While *V. fischeri* is solitary and expresses polar flagella in seawater, upon encountering
89 the juvenile bobtail squid light organ the bacteria require the symbiosis polysaccharide (Syp) to
90 aggregate in the host mucus prior to commencing further colonization (Koehler et al., 2019;
91 Rotman et al., 2019; Ruby and Asato, 1993; Yip et al., 2006, 2005). The bacterial aggregates
92 form on the outer face of the light organ independent of flagellar motility and are influenced by
93 physical currents generated by cilia on the light organ surface (Nawroth et al., 2017; Nyholm et
94 al., 2000). Host-produced nitric oxide stimulates dispersal from the biofilm aggregates
95 (Thompson et al., 2019), and the bacteria swim through the pore into the light organ ducts using
96 flagellar motility and chemotaxis toward squid-derived chitin oligosaccharides (Brennan et al.,
97 2013b; Graf et al., 1994; Mandel et al., 2012; Millikan and Ruby, 2002; Ruby and Asato, 1993).
98 The symbionts pass through an antechamber and bottleneck before reaching the crypts of the
99 light organ, where they reach high density and produce light to camouflage the shadow of the
100 squid host (Jones and Nishiguchi, 2004; McFall-Ngai and Ruby, 1991; Sycuro et al., 2006). The
101 initiation of this process—including biofilm formation, chemotaxis, and motility—occurs only
102 when the squid is newly hatched, as colonizing bacteria seed the host for its lifetime. Therefore,
103 the mechanisms that regulate these processes are fundamental to selection for the correct
104 symbionts and the establishment of the association.
105
106 As with the pathogens noted above, *V. fischeri* (strain ES114) encodes a large number of
107 proteins predicted to regulate c-di-GMP levels: 50 total that encompass 28 DGCs, 14 PDEs, 5
108 DGC/PDEs, and 3 proteins that are predicted to be degenerate (Wolfe and Visick, 2010). Roles
109 for DGCs MifA and MifB, and PDEs BinA and PdeV in *V. fischeri* motility and/or biofilm
110 formation have been described (Bassis and Visick, 2010; Christensen et al., 2020; O'Shea et

111 al., 2006). However, those studies did not examine individual mutants during squid colonization,
112 and a large-scale transposon-insertion sequencing study did not identify individual mutations in
113 genes related to c-di-GMP that were predicted to have significant phenotypes in the squid host
114 (Brooks et al., 2014). Given the predicted complexity of the c-di-GMP network in *V. fischeri*, we
115 used new technology (Visick et al., 2018) to generate strains lacking multiple DGCs or PDEs to
116 mimic either low or high c-di-GMP levels, and we applied these strains to determine the effects
117 of c-di-GMP extremes on squid colonization. This approach allowed us to directly study the role
118 of c-di-GMP *in vivo* during beneficial colonization, to determine bacterial behaviors that are
119 influenced by the compound during animal colonization, and to reveal signaling interactions that
120 are not evident during growth in culture.
121
122 **RESULTS**
123
124 **Deletion of multiple DGCs or PDEs effectively manipulates c-di-GMP levels in the**
125 **symbiont *V. fischeri***
126 To determine the role that c-di-GMP plays during the beneficial colonization of *E. scolopes* by *V.*
127 *fischeri*, we constructed strains that were altered in their basal levels of c-di-GMP. While it is not
128 yet feasible to delete all 50 c-di-GMP-related genes in a single strain, we applied recently
129 developed technology that facilitates rapid construction of multiple gene deletions *(Visick et al.,*
130 *2018)* to generate a strain that lacked seven DGCs (Δ7DGC; lacking *VF_1200*, *mifA*, *VF_1245*,
131 *VF_A0342-A0343*, *VF_1639*, and *VF_A0216*) and another that lacked six PDEs (Δ6PDE;
132 lacking *pdeV*, *VF_2480*, *binA*, *VF_0087*, *VF_1603*, and *VF_A0506*). These genes were targeted
133 based on preliminary experiments assessing the importance of individual genes in biofilm
134 formation, primarily the control over cellulose production (via Congo red binding), a c-di-GMP-
135 dependent phenotype (Bassis and Visick, 2010). We examined the levels of c-di-GMP in these
136 strains using the pFY4535 c-di-GMP reporter (Zamorano-Sánchez et al., 2019) and determined

137 that the Δ7DGC strain had c-di-GMP levels over 9-fold lower than the parent strain, while the
138 Δ6PDE strain exhibited c-di-GMP levels about 1.5-fold higher (**Fig. 1A**). These differences were
139 observed in rich medium as well as in artificial seawater (**Fig. 1A**), suggesting to us that these
140 strains would be effective for studying the role of c-di-GMP during squid colonization. We
141 examined phenotypes known to be regulated by c-di-GMP, including cellulose biofilm formation
142 and flagellar motility. The Δ7DGC strain displayed elevated motility on TBS soft agar, reduced
143 Congo red binding, and reduced activity of a *bcsQ'-gfp*$^{+}$ cellulose locus transcriptional reporter
144 (**Fig. 1B-D**). The Δ6PDE strain exhibited the opposite phenotypes (**Fig. 1B-D**). These data
145 supported our contention that we could use the multiple deletion approach to examine c-di-GMP
146 regulation in the symbiont. Together, these data and those below support that the Δ7DGC strain
147 represents cells in a low c-di-GMP state whereas the Δ6PDE cells are in a high c-di-GMP state,
148 and for the remainder of the study we will refer to these strains as the "Low cdG" and "High
149 cdG" strains, respectively.
150

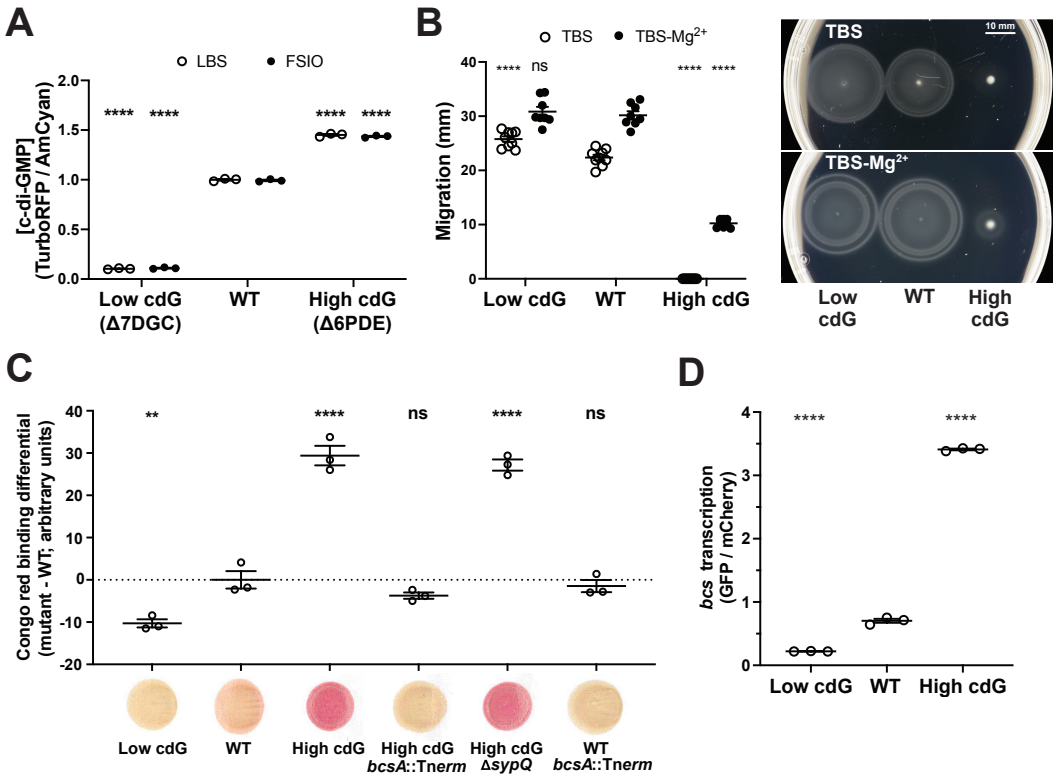

Fig. 1. High c-di-GMP levels inhibit swimming motility, promote Congo red binding, and promote cellulose gene transcription. (A) Quantification of c-di-GMP concentration for *V. fischeri* and indicated mutants using the pFY4535 c-di-GMP reporter plasmid. For each strain, n = 3 biological and n = 3 technical replicates, each point represents the mean of technical replicates, average bars represent the mean of biological replicates, and error bars represent standard error of the mean. (B) Quantification of migration through soft (0.3%) agar for *V. fischeri* and indicated mutants. For each strain, n = 8-9 biological replicates, average bars represent mean, and error bars represent standard error of the mean. Motility plate images are representative. (C) Quantification of Congo red binding for *V. fischeri* and indicated mutants. For each strain, n = 3 technical replicates, average bars represent mean, and error bars represent standard error of the mean. Congo red spot images are representative. (D) Quantification of *in vitro bcs* transcription by *V. fischeri* and indicated mutants using the pRYI063 *bcsQ-gfp*$^{+}$ transcriptional reporter plasmid. For each strain, n = 3 biological replicates. Points represent each biological replicate, average bars represent the mean, and error bars represent standard error of the mean. For A-D, one-way ANOVA was used for statistical analysis and asterisks represent significance relative to the WT strain; ns = not significant, *$p < 0.05$, **$p < 0.006$, ****$p < 0.0001$.

Elevated c-di-GMP levels interfere with productive colonization initiation

To determine whether the lower and/or higher c-di-GMP levels impacted symbiotic colonization, we introduced the Low cdG and High cdG strains to newly hatched *E. scolopes* squid. Each strain was individually inoculated into a bowl with hatchling squid and allowed to initiate colonization for 3 h. The squid were transferred to new water, and the bacterial load in each

159 host was measured at 18 and 48 hours-post-inoculation (hpi) (Naughton and Mandel, 2012). For
160 WT *V. fischeri* ES114, this process leads to approximately 10^5 CFU per squid at 18 and 48 hpi,
161 and a similar yield was observed for the Low cdG strain (**Fig. 2**). This was surprising to us,
162 given that there are 50 genes that encode c-di-GMP synthesis/degradation factors, yet
163 downregulation of c-di-GMP levels by over 9-fold did not impact the ability to colonize the squid
164 host (**Fig. 2**). To ask whether the low cdG strain exhibited a more subtle colonization defect that
165 we were not detecting in this single strain colonization assay, we performed a competitive
166 colonization assay in which the Low cdG and WT strain were co-inoculated. We reasoned that if
167 the Low cdG strain had a slight defect in the host, then the competitive assay could reveal this
168 effect. However, in the competitive assay, the Low cdG strain exhibited similar fitness as the WT
169 strain (**SFig. 1**). In contrast, in the single-strain colonization assay, the High cdG strain had a
170 substantial deficit in bacterial yield in the host as early as 18 hpi and also at 48 hpi, with a
171 median CFU below 10^3 per light organ (**Fig. 2**). In the competitive colonization, the High cdG
172 strain displayed a significant deficit, as WT outcompeted the High cdG strain by over 3000-fold
173 (**SFig. 1**). Growth of the High cdG strain in culture was similar to WT (**SFig. 2**), arguing that the
174 colonization defect is due to a developmental deficit in the host and not an inherent growth
175 property of the strain. From these data, we conclude that high levels of c-di-GMP are
176 detrimental for the initiation of a beneficial colonization in the squid light organ, whereas low
177 levels of c-di-GMP do not impact the colonization behavior during the first 48 h of symbiosis.

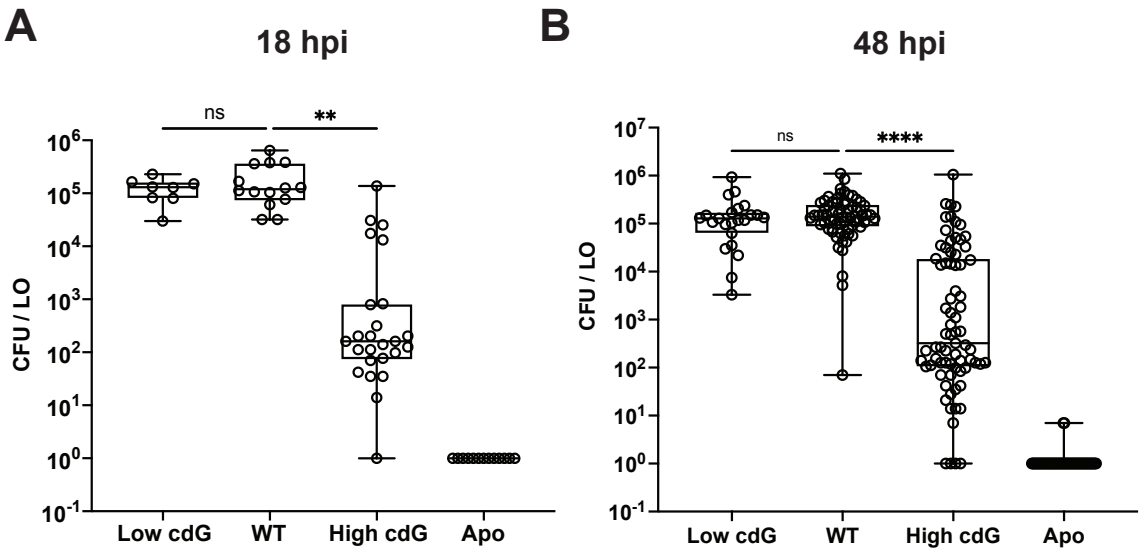

178

Fig. 2. Elevated c-di-GMP levels inhibit host colonization. (A) Quantification of squid colonization levels at 18 hpi by *V. fischeri* and indicated mutants. Sample sizes from left to right are 8, 14, 25, and 13 squid. (B) Quantification of squid colonization levels at 48 hpi by *V. fischeri* and indicated mutants. Sample sizes from left to right are 23, 68, 75, and 65 squid. For A and B, box-and-whisker plots represent minimum, 25th percentile, median, 75th percentile, and maximum. Kruskal-Wallis test was performed for statistical analysis for squid that were introduced to bacteria; ns = not significant, **$p < 0.002$, ****$p < 0.0001$.

179

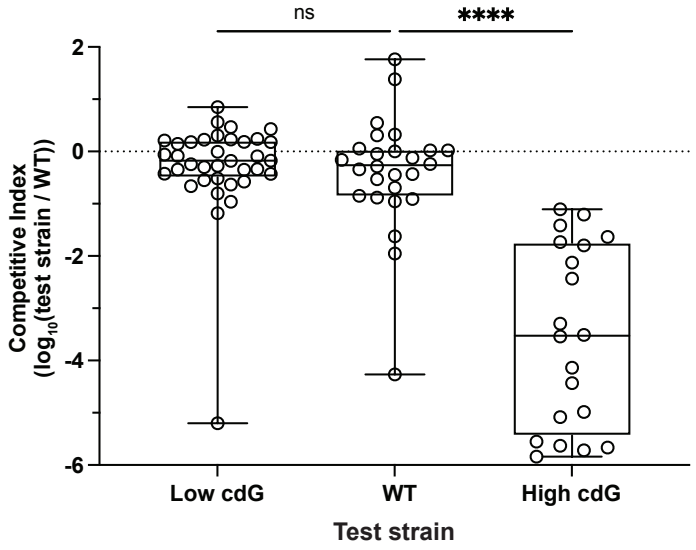

180

Supp. Fig. 1. Low levels of c-di-GMP do not inhibit host colonization. Quantification of squid competitive colonization index at 48 hpi by the indicated *V. fischeri* mutants. Competitive index represents $\log_{10}((\text{test strain/WT})_{output}/ (\text{test strain/WT})_{input})$. Box-and-whisker plots represent minimum, 25th percentile, median, 75th percentile, and maximum. Sample sizes from left to right are 36, 26, and 20 squid. Kruskal-Wallis test was performed for statistical analysis; ns = sot significant, ****$p < 0.0001$.

181

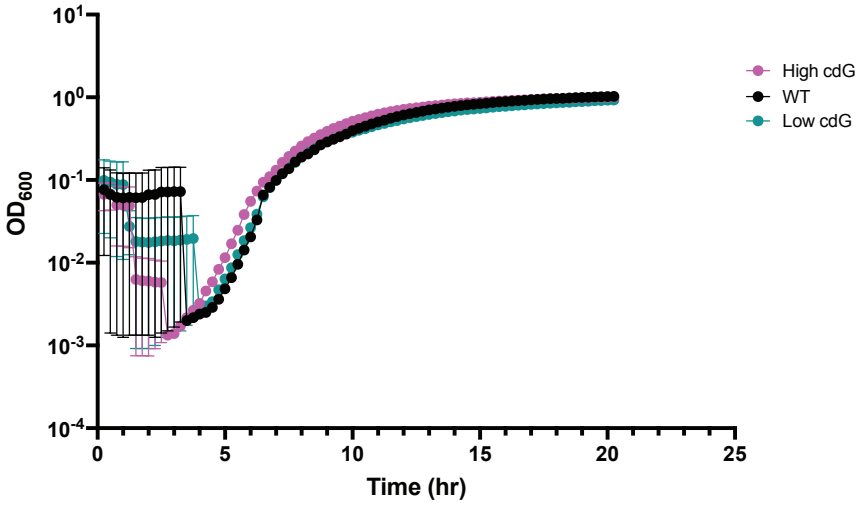

182

Supp. Fig. 2. The High c-di-GMP *V. fischeri* strain does not have a growth defect. Growth curves for *V. fischeri* and indicated mutants. For each strain, n = 3 biological and n = 6 technical replicates. Points represent the mean of biological replicates. Error bars represent standard error of the mean. Doubling time during exponential phase for High cdG is 30.4 minutes, for WT is 27.4 minutes, and for Low cdG is 31.9 minutes.

183

184 To ask whether the phenotypes we observed in the High cdG strain were due to regulation of c-
185 di-GMP levels or whether they were due to a specific gene product that is absent (i.e., signaling
186 specificity), we introduced a PDE from *V. cholerae*, VC1086, that is known to be active in
187 heterologous bacteria (Spurbeck et al., 2012; Waters et al., 2008), and that we predicted would
188 lower c-di-GMP levels in *V. fischeri*. Across the phenotypes tested, the plasmid-expressed
189 VC1086 had only a slight effect in a WT background (**Fig. 3**). However, in the High cdG
190 background, expression of VC1086 reduced cdG levels by 1.6-fold, restored swimming motility
191 on TBS agar, and reduced Congo red binding 1.7-fold in the High cdG background (**Fig. 3A-C**).
192 In a squid colonization assay, expression of the *V. cholerae* PDE rescued colonization of the
193 High cdG strain (**Fig. 3D**). This result argues that the squid colonization defect observed in the
194 High cdG strain is a result of the altered c-di-GMP levels and not due to the absence of a
195 specific *V. fischeri* protein. This set of experiments confirmed that our results were due to
196 altering levels of c-di-GMP rather than the absence of a single gene product. We conclude that
197 lower levels of c-di-GMP are not harmful to establishing a symbiotic association, while higher
198 levels are detrimental to symbiotic initiation.

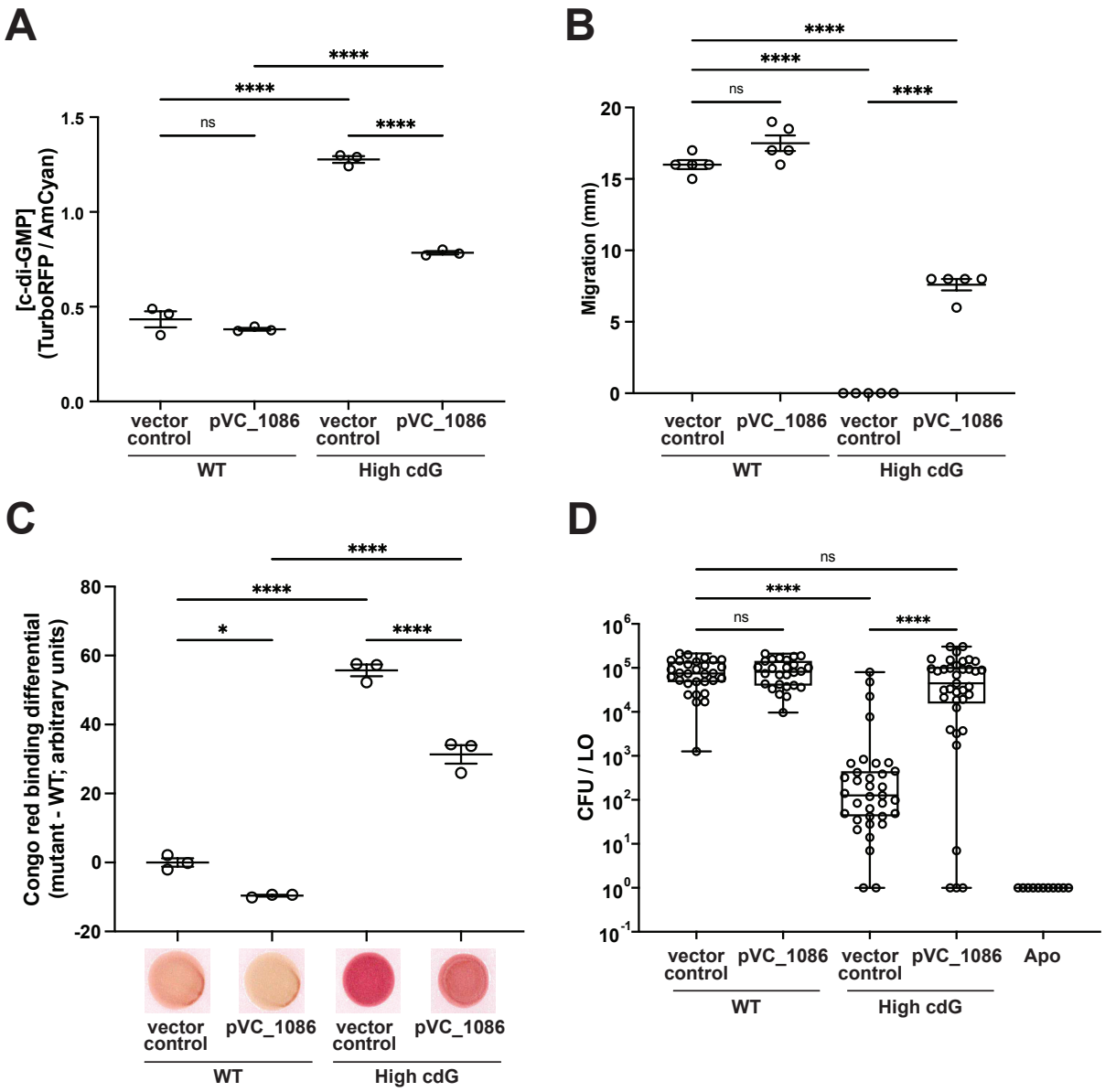

Fig. 3. Reduced swimming motility, increased Congo red binding, and diminished squid colonization of the High cdG strain are dependent on high c-di-GMP levels. (A) Quantification of c-di-GMP concentration for *V. fischeri* and indicated mutants using the pFY4535 c-di-GMP reporter plasmid. For each strain, n = 3 biological and n = 3 technical replicates, each dot represents mean of technical replicates, average bars represent the mean of biological replicates, and error bars represent standard error of the mean. (B) Quantification of migration through TBS soft (0.3%) agar for *V. fischeri* and indicated mutants. For each strain, n = 5 biological replicates, average bars represent mean, and error bars represent standard error of the mean. (C) Quantification of Congo red binding for *V. fischeri* and indicated mutants. For each strain, n = 3 technical replicates, average bars represent the mean, and error bars represent standard error of the mean. Congo red spot images are representative. For A-C, one-way ANOVA was used for statistical analysis; ns = not significant, *p = 0.017, ****p < 0.0001. (D) Quantification of squid colonization levels at 48 hpi by *V. fischeri* and indicated mutants. Box-and-whisker plots represent minimum, 25th percentile, median, 75th percentile, and maximum. Sample sizes from left to right are 30, 26, 34, 37, and 11 squid. Kruskal-Wallis test was performed for statistical analysis for squid that were introduced to bacteria; ns = not significant, ****p < 0.0001.

201 **The High c-di-GMP strain exhibits flagellar motility *in vivo***

202

203 In culture, the High cdG strain had a substantial swimming motility defect (**Fig. 1B**). We
204 therefore considered the hypothesis that a key basis for the poor colonization by the High cdG
205 strain was due to the altered flagellar motility, which is required for host colonization (Brennan et
206 al., 2013b; Millikan and Ruby, 2002; Ruby and Asato, 1993). In culture, we did observe a
207 migration ring, demonstrating that the strain is not amotile (**Fig. 1B**). Cells from the outer ring of
208 motility from the High cdG strain (**Fig. 1B**) retained their phenotype upon reinoculation into a
209 new plate, arguing that the motility observed was not due to spontaneous suppressor mutants.
210 At the same time, we observed that the motility detected was dependent on the media used,
211 with higher motility being observed in the presence of magnesium sulfate (**Fig. 1B**) (O'Shea et
212 al., 2005). An open question, then, was whether this strain exhibited flagellar motility under the
213 conditions experienced in the light organ mucus. We therefore performed a competitive
214 colonization assay between the High cdG strain and the amotile High cdG Δ*flrA* isogenic
215 derivative. The High cdG strain outcompeted the amotile Δ*flrA* derivative, with a median
216 advantage of approximately 10-fold (**Fig. 4**), supporting that the High cdG strain is indeed motile
217 in the host.

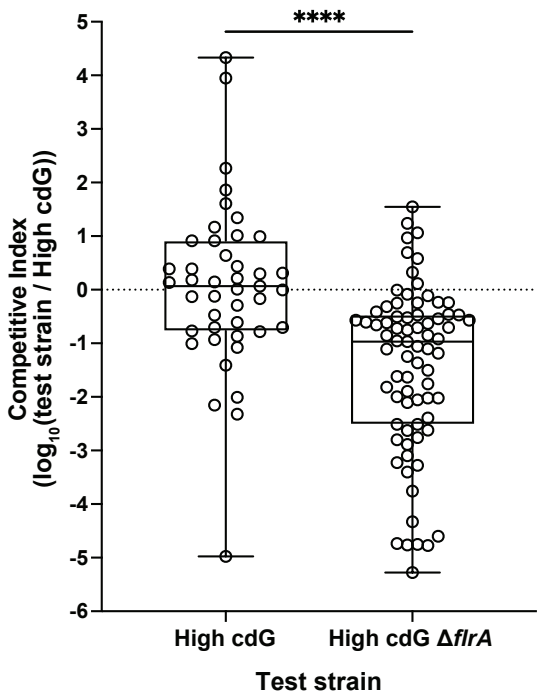

Fig. 4. High c-di-GMP levels do not eliminate motility during host colonization. Quantification of squid competitive colonization index at 48 hpi by the indicated *V. fischeri* mutants. Competitive index represents $\log_{10}((\text{test strain/High cdG})_{output}/(\text{test strain/High cdG})_{input})$. Box-and-whisker plots represent minimum, 25th percentile, median, 75th percentile, and maximum. Sample sizes from left to right are 43 and 75 squid. Kruskal-Wallis test was performed for statistical analysis; ****$p < 0.0001$.

Elevated c-di-GMP levels lead to altered aggregate morphology *in vivo*

The *V. fischeri*-squid system provides an opportunity to combine genetic and imaging approaches to study the planktonic-to-biofilm transition during colonization of a symbiotic host. Symbiosis polysaccharide (Syp) is required for host colonization (Yip et al., 2006), while the distinct cellulose polysaccharide is not known to impact host phenotypes, so we questioned whether c-di-GMP would impact Syp-dependent aggregation *in vivo*. At 3 hpi, we examined *in vivo* biofilm aggregates using *V. fischeri* that constitutively expressed a fluorescent protein (GFP or mCherry). Compared to the Low cdG strain, the High cdG strain produced larger-sized aggregates, while the WT aggregates were an intermediate size (**Fig. 5A,B**). In over 10% of the light organs examined, the High cdG strain had four or more aggregates, which were not observed in the WT strain (**Fig. 5C**).

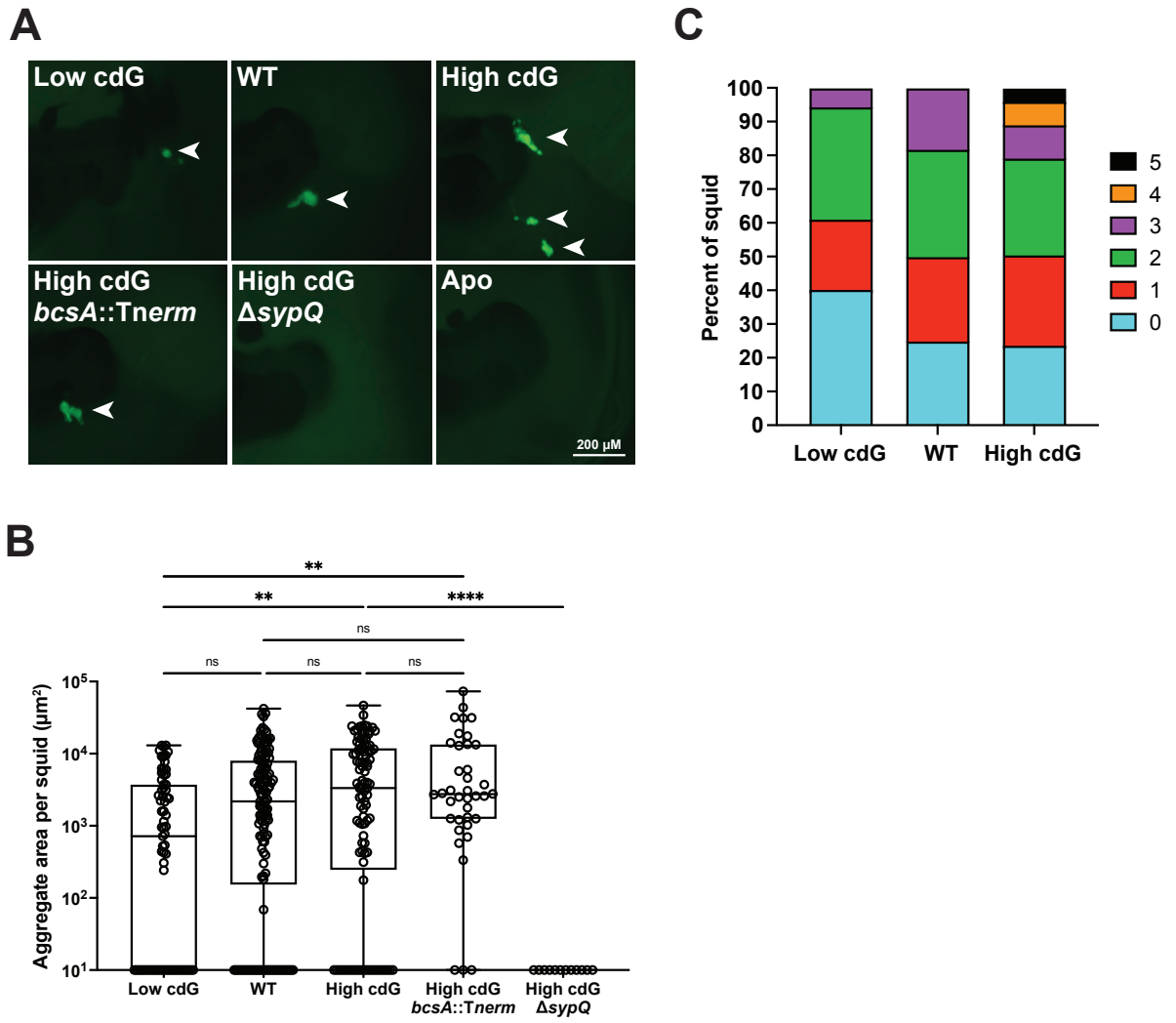

232

Fig. 5. Elevated c-di-GMP levels lead to a greater number of *V. fischeri* aggregates in the squid host. (A) Representative fluorescence microscopy images of aggregates made by *V. fischeri* and indicated mutants carrying a constitutive GFP on the pVSV102 plasmid within the host mucus. Arrows indicate location of aggregates. (B) Quantification of aggregate area per squid for *V. fischeri* and indicated mutants carrying a constitutive GFP on the pVSV102 plasmid. Samples sizes from left to right are 73, 134, 101, 38, and 12 squid. Kruskal-Wallis test was used for statistical analysis; ns = not significant, **$p < 0.02$, ****$p < 0.0001$. (C) Quantification of number of *V. fischeri* aggregates formed per squid. Box-and-whisker plots represent minimum, 25th percentile, median, 75th percentile, and maximum. Samples sizes from left to right are 73, 134, and 101 squid.

233

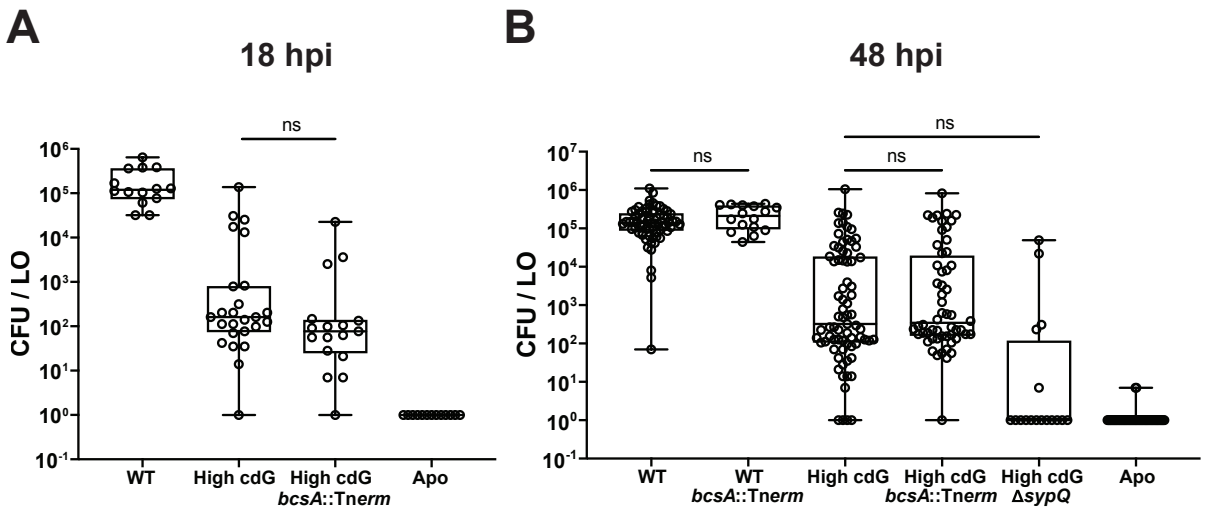

Supp. Fig. 3. Absence of the cellulose synthase BcsA does not rescue the high c-di-GMP strain colonization defect. (A) Quantification of squid colonization levels at 18 hpi by *V. fischeri* and indicated mutants. Sample sizes from left to right are 14, 25, 17, and 13 squid. (B) Quantification of squid colonization levels at 48 hpi by *V. fischeri* and indicated mutants. Sample sizes from left to right are 68, 16, 75, 56, 17, and 65 squid. For A and B, data for WT, High cdG, and Apo groups are the same as in Fig. 2. Box-and-whisker plots represent minimum, 25th percentile, median, 75th percentile, and maximum. Kruskal-Wallis test was performed for statistical analysis for squid that were introduced to bacteria; ns = not significant.

To test if the Syp polysaccharide was required for the pattern of multiple bacterial aggregates we observed in the High cdG strain, we deleted the gene encoding the structural Syp protein SypQ in the High cdG background. This strain failed to colonize the host robustly at 48 hpi (**SFig. 3B**) and did not form detectable aggregates (**Fig. 5A,B**), demonstrating that Syp-dependent biofilm is required for *in vivo* aggregation in the High cdG background. We asked whether transcription of the *syp* locus was altered in the High cdG strain. Activity of a *sypA'-gfp*$^+$ reporter was examined during the aggregation phase, where we found that in the host, *sypA* transcription was substantially reduced in the High cdG strain compared to the WT parent (**Fig. 6A, SFig. 4A**). High levels of c-di-GMP therefore negatively impact the expression of the symbiosis polysaccharide locus *in vivo*. Notably, when we asked whether the High cdG strain had altered *syp* transcription *in vitro*, we found no significant effects under two different media conditions (**Fig. 6C**). Therefore, c-di-GMP exerts a host-specific effect on symbiotic biofilm expression.

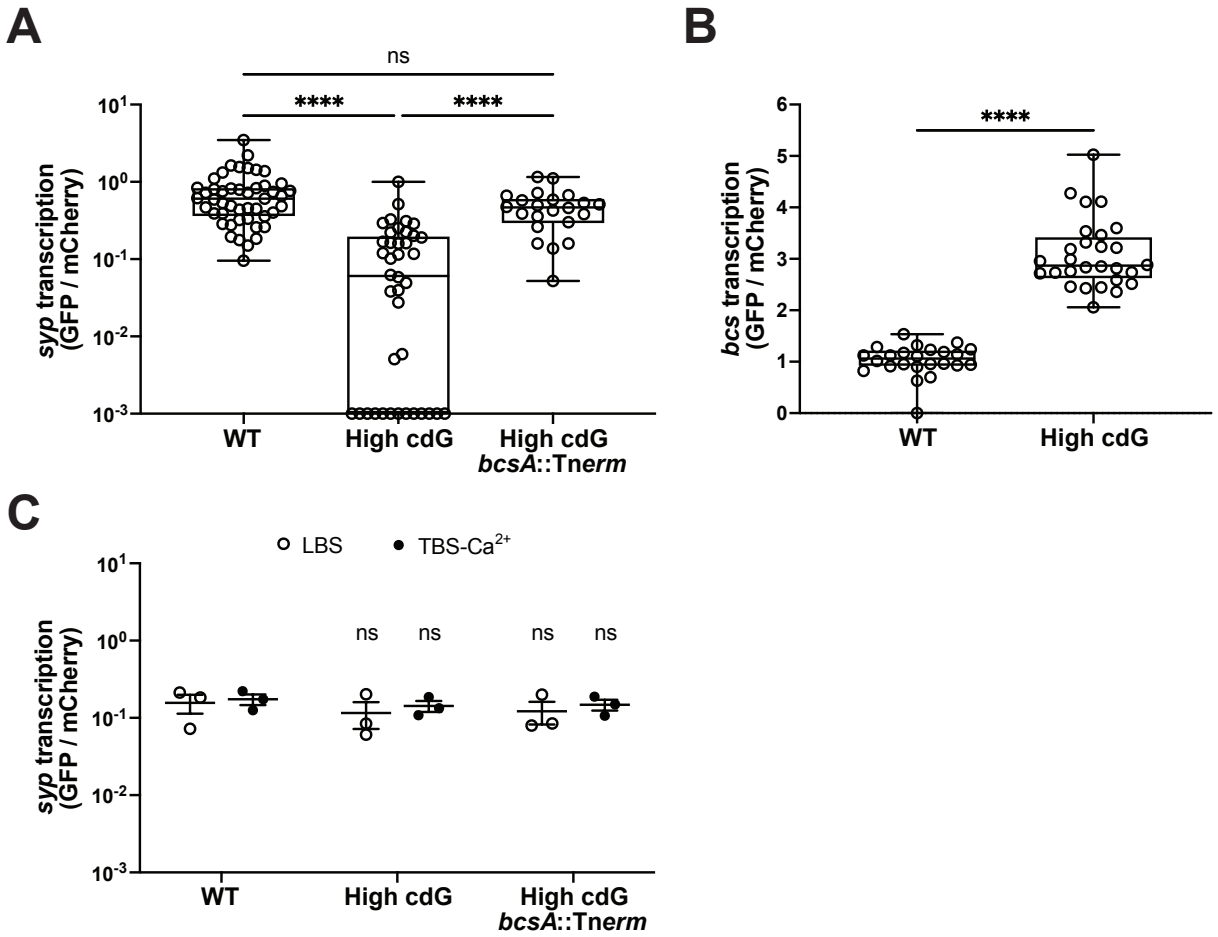

Fig. 6. c-di-GMP downregulates *syp* via BcsA in host mucus but not in culture. (A) Quantification of *syp* transcription for *V. fischeri* and indicated mutants using the pM1422 *sypA*'-*gfp*$^+$ transcriptional reporter plasmid in aggregates within the host mucus. Samples sizes from left to right are 47, 40, and 22 aggregates. (B) Quantification of *bcs* transcription for *V. fischeri* and indicated mutants using the pRYI063 *bcsQ*'-*gfp*$^+$ transcriptional reporter plasmid in aggregates within the host mucus. Samples sizes from left to right are 24 and 28 aggregates. For A and B, Box-and-whisker plots represent minimum, 25th percentile, median, 75th percentile, and maximum. Kruskal-Wallis test was used for statistical analysis; ns = not significant, ****$p < 0.0001$. (C) Quantification of *in vitro syp* transcription in LBS and TBS-Ca^{2+} for *V. fischeri* and indicated mutants carrying the pM1422 *sypA*'-*gfp*$^+$ transcriptional reporter plasmid. For each strain, n = 3 biological replicates. Points represent each replicate, average bars represent the mean of replicates, and error bars represent the standard error of the mean. One-way ANOVA was used for statistical analysis; ns = not significant relative to the WT strain in the same media.

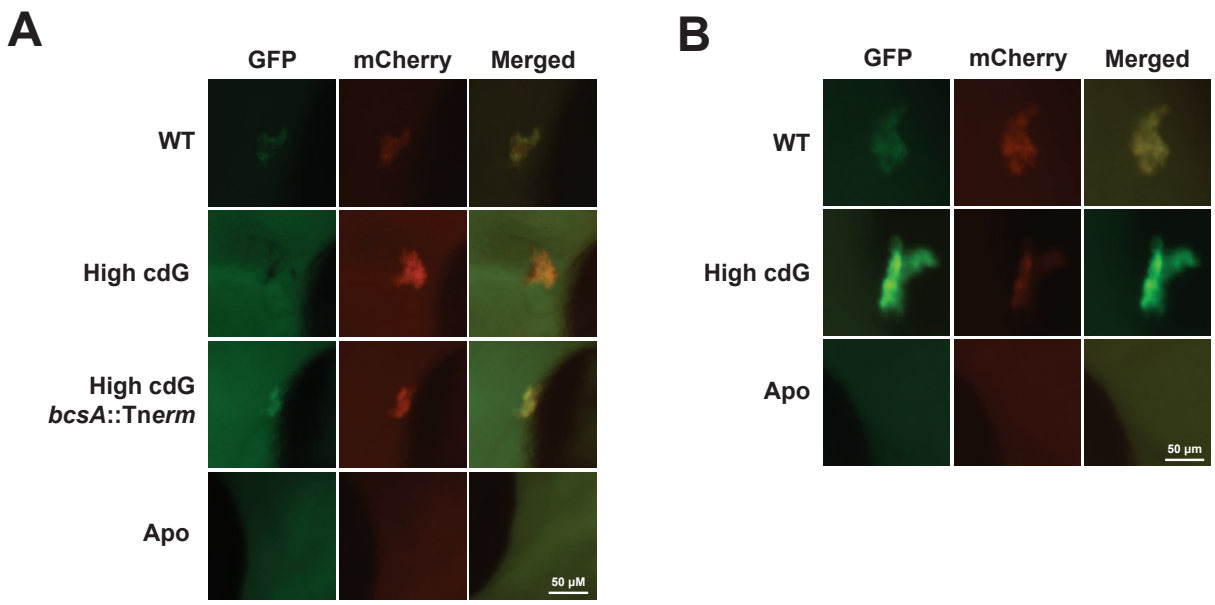

251

Supp. Fig. 4. High c-di-GMP-dependent *bcs* expression inhibits *syp* expression in bacterial aggregates within the host mucus. (A) Representative fluorescent microscopy images of squid light organs containing *V. fischeri* and indicated mutants carrying the pM1422 *sypA*'-*gfp*$^{+}$ transcriptional reporter plasmid. (B) Representative fluorescent microscopy images of squid light organs containing *V. fischeri* and indicated mutants carrying the pRYI063 *bcsQ*'-*gfp*$^{+}$ transcriptional reporter plasmid.

252

253

254 **High levels of c-di-GMP repress *syp* polysaccharide transcription via the cellulose**

255 **polysaccharide and in a host-dependent manner**

256

257 In previous studies in the squid host, larger bacterial aggregates have correlated with an

258 upregulation of *syp* gene transcription and a higher propensity for colonization initiation and

259 competitive fitness (Brooks and Mandel, 2016; Morris et al., 2011; Yip et al., 2006). In this case,

260 however, the larger aggregates of the High cdG strain have reduced *syp* transcription and

261 exhibit poor colonization (**Fig. 6A, SFig. 4A, Fig. 2**). We therefore asked if there was another

262 component of the aggregate that may contribute to the morphology observed but that may not

263 enhance colonization ability in the same way that additional Syp polysaccharide promotes

264 colonization. A candidate for this component is cellulose, as we demonstrated above that

265 cellulose is upregulated in the High cdG strain (**Fig. 1C,D**). Therefore, we asked whether there

266 may be an interaction between the cellulose and Syp polysaccharide biosynthetic pathways. We
267 measured *bcsQ* transcription *in vivo* using a fluorescent transcriptional reporter (*bcsQ'-gfp*$^+$),
268 and we determined that *bcsQ* transcription was elevated in bacterial aggregates in the host
269 mucus in the High cdG strain compared to WT (**Fig. 6B, SFig. 4B**). Using a *bcsA*::Tn*erm*
270 transposon insertion mutant that interrupts cellulose synthase, we examined colonization in the
271 context of the High cdG background. Interruption of *bcsA* did not improve colonization at 18 or
272 48 hpi compared to the High cdG strain (**SFig. 3**). However, compared to the High cdG strain, a
273 *bcsA* derivative exhibited higher *sypA'-gfp*$^+$ transcription *in vivo* (**Fig. 6A, SFig. 4A**), yet no
274 difference in *sypA'-gfp*$^+$ transcription was observed *in vitro* with the same strains (**Fig. 6C**).
275 These data present a novel connection between transcriptional control of polysaccharide
276 systems that occurs specifically in the host.
277
278 **DISCUSSION**
279
280 **Cyclic di-GMP impacts multiple pathways during beneficial colonization.** Our study was
281 motivated by the question of how c-di-GMP impacts a beneficial microbe-host association. To
282 ask this question, we focused on the *V. fischeri*-squid mutualism. This well-studied binary
283 association allows us to examine individual stages of colonization using strains deleted for 6-7
284 genes and that consequently have altered levels of c-di-GMP. We found that a strain with
285 elevated levels of c-di-GMP exhibited striking defects during host colonization. The High cdG
286 strain formed aggregates that trended larger (**Fig. 4**), had altered host-specific polysaccharide
287 gene expression in the aggregates (**Fig. 6A,B, SFig. 4**), exhibited reduced flagellar motility (**Fig.
288 1B**), and displayed a significant colonization defect as enumerated by bacterial counts in the
289 host as early as 18 hpi (**Fig. 2**). Colonization of the High cdG strain was rescued by
290 overexpression of a heterologous PDE that does not have significant homology to proteins in *V.*

291 *fischeri* (**Fig. 3D**), strongly supporting that the observed effects are due to the c-di-GMP levels
292 and not to individual functions of the gene products affected in the multiple deletion strains.
293
294 Our results parallel work in several pathogenic bacteria, where constitutively elevated c-di-GMP
295 levels are correlated with a decrease in virulence (Hall and Lee, 2018; Römling et al., 2013). In
296 *V. cholerae*, for example, elevated c-di-GMP led to 5-fold reduced competitive colonization in
297 the infant mouse small intestine model (Tamayo et al., 2008). In that study, the authors tested if
298 the reduction was due to overexpression of biofilm (VPS), but it was not, and they attributed the
299 phenotype to the resulting virulence gene expression downstream of c-di-GMP. We note that
300 the magnitude of the effect we observe in *V. fischeri* colonization of bobtail squid is substantially
301 higher: >100-fold in a single-strain colonization assay. It therefore seems likely that this aspect
302 of mutualism is broadly shared with pathogenic colonization, and we expect there to be strong
303 constraints to retain c-di-GMP levels low during the initiation of the host colonization process.
304 There are also likely to be beneficial symbiosis-specific adaptations within c-di-GMP signaling.
305 For example, the zebrafish gut symbiont *Aeromonas veronii* responds to host amino acids to
306 inhibit a diguanylate cyclase, thereby stimulating bacterial motility into the host (Robinson et al.,
307 2021). It remains to be seen whether there are similar specific adaptations in the *V. fischeri*-
308 squid symbiosis.
309
310 Despite encoding 50 genes that manipulate c-di-GMP, we were surprised to find that
311 substantially lowering levels of c-di-GMP (approximately 9-fold) (**Fig. 1A**) led to no significant
312 defect in host colonization. In the Low cdG strain, we detected slightly smaller bacterial
313 aggregates in the host mucus (**Fig. 5**), but no consequent diminution of bacterial counts in the
314 light organ at 18 hpi or 48 hpi (**Fig. 2**). The Low cdG strain similarly exhibited no competitive
315 colonization defect (**SFig. 1**). When examining transcriptional reporters for the symbiosis
316 polysaccharide gene *sypA* or the cellulose biosynthesis gene *bcsQ in vivo*, the Low cdG strain

317 resembled the wild-type parent (**Fig. 6A,B, SFig. 4**). We note that colonization was intact
318 despite this strain exhibiting strong biofilm and motility phenotypes *in vitro* (**Fig. 1**), thus
319 emphasizing the importance of studying these phenotypes in the relevant host system.
320
321 It seems likely that the squid host environment may influence c-di-GMP levels during
322 colonization. Our transcriptional reporter data support this contention. In culture, we observed a
323 3.2-fold increase in *bcsQ'-gfp*$^{+}$ reporter expression in the WT strain relative to the Low cdG
324 strain (**Fig. 1D**). However, in the animal, we observed similar *bcsQ* expression in the two strains
325 (**Fig. 6B, SFig. 4B**), suggesting that the lower *bcsQ* expression of the WT strain occurs in
326 response to the host environment. Similarly, the upregulation of *bcs* gene expression due to
327 elevated c-di-GMP conditions resulted in a substantial downregulation of *sypA'-gfp*$^{+}$ in the host,
328 yet no comparable effect was observed under two distinct culture conditions (**Fig. 6**). Given the
329 multiple cases in which gene expression in the host is distinct from that observed in culture, it
330 remains an intriguing question as to how the host influences bacterial c-di-GMP signaling and
331 the downstream pathways.
332
333 If the Low cdG strain thrives in the host, is c-di-GMP required for *V. fischeri* biology in the squid?
334 Given that there are another twenty-one DGCs and five putative bifunctional DGC/PDEs still
335 present in the Low cdG strain, our results do not preclude a requirement for c-di-GMP during
336 colonization. It remains possible that additional DGCs perform localized functions that were not
337 addressed in the current study and/or that DGCs play critical roles at later stages in the
338 colonization process.
339
340 **Construction of multiple-gene deletions in *V. fischeri* is an effective tool to tackle gene**
341 **families.** The recent development of a method for construction of serial deletions (Visick et al.,
342 2018) enabled the construction of multiple-mutant strains such as the Low cdG and High cdG

343 strains in this study. We have further extended the method to allow for detection of barcoded
344 deletions in competitive colonization experiments (Burgos et al., 2020). The work in this study
345 highlights the utility of such approaches to interrogate gene families. There are many instances
346 in which deletions of multiple genes could clarify the role of various biological processes.
347 Previously, we identified a role for chemotaxis toward chitin oligosaccharides as a key
348 developmental stage during squid colonization (Mandel et al., 2012). Efforts from our group and
349 others have studied 23 *V. fischeri* chemoreceptors through a combination of single and multiple
350 mutants (Bennett et al., 2020; Brennan et al., 2013a; Nikolakakis et al., 2015), but there are a
351 total of 43 methyl-accepting chemoreceptors encoded in the ES114 genome, and the
352 receptor(s) for chitin oligosaccharides remain elusive. Generation of multiple mutant strains has
353 been especially valuable to dissect gene families in *V. cholerae* (Hayes et al., 2017), and our
354 work suggests that a similar approach will be useful in *V. fischeri*.
355
356 **Elevated c-di-GMP levels diminish, but do not eliminate, flagellar motility *in vivo***
357 The High cdG strain has a significant soft agar motility defect (**Fig. 1B**), and amotile strains are
358 at a significant colonization disadvantage compared to WT. Our competition of the High cdG
359 strain with the isogenic Δ*flrA* derivative revealed a 15-fold advantage for the former during squid
360 colonization (**Fig. 4**). Our interpretation of this result is that the High cdG strain retains the ability
361 to be motile in the host despite the elevated c-di-GMP levels. The magnitude of the competitive
362 advantage (15-fold) is diminished compared to that of the wild-type strain competing against a
363 Δ*flrA* strain (>1,000-fold) (Burgos et al., 2020; Millikan and Ruby, 2003). Therefore, it seems
364 likely that c-di-GMP does impact motility in the host, but not to the extent that it fully prohibits
365 colonization.
366
367 **Cyclic di-GMP has a qualitative effect on the nature of the exopolysaccharide in animal**
368 **tissue.** The increased number of aggregates observed in the High cdG strain in squid is, to our

369 knowledge, the first time such a phenotype has been observed (**Fig. 5**). Hypermotile mutants
370 were noted to exhibit more diffuse aggregates on the light organ surface, though these were
371 often smaller than their WT counterparts (Millikan and Ruby, 2002). Multiple studies have noted
372 larger *in vivo* aggregates upon overexpression of biofilm activator RscS or removal of biofilm
373 inhibitor BinK (Brooks and Mandel, 2016; Yip et al., 2006). In both cases, it was shown that Syp
374 was the relevant pathway induced, and the cells within the resulting larger aggregates were
375 functional to outcompete those from WT aggregates. The morphology and gene expression in
376 High cdG aggregates are significantly more complicated and implicate an interaction between
377 cellulose and Syp exopolysaccharides. We showed that cellulose on its own is not required for
378 colonization (**SFig. 3B**). However, the high c-di-GMP condition revealed a role for the *bcs*
379 (cellulose synthase) locus in regulating *syp* (mirroring results obtained in specific agar
380 conditions in (Dial et al., 2021b)) (**Fig. 6A, SFig. 4A**). Therefore, while cellulose production on
381 its own does not impact colonization, in the High cdG background it significantly impacts
382 expression of *syp*. In *Pseudomonas aeruginosa*, roles for multiple exopolysaccharide systems in
383 biofilm formation have been explored, for example as the Psl and Pel systems have distinct but
384 also overlapping roles in attachment and biofilm formation (Colvin et al., 2012). In *V. fischeri*,
385 our work supports data in the literature that Syp is the key system for *in vivo* biofilm formation
386 and that the cellulose system is dispensable for host colonization. At the same time, this study
387 reveals a novel transcriptional interaction among two exopolysaccharide systems. This interplay
388 may impact the formation of multiple-exopolysaccharide biofilms during later stages of host
389 colonization or under environmental conditions that have yet to be explored, and points to a
390 novel regulatory mechanism that connects biofilm regulation in an animal host.
391
392 In conclusion, this work identified a role for c-di-GMP regulation during the initiation of a
393 mutualism, identified specific developmental stages in the host that were regulated by altered c-
394 di-GMP levels, and revealed a transcriptional interplay between multiple exopolysaccharide

395 systems that is apparent only in the host. Our study therefore lays the groundwork for future
396 investigations into how this widespread bacterial compound influences bacterial behaviors
397 beyond pathogenesis to impact microbiome behavior and interactions with symbiotic hosts.
398

399 **MATERIALS AND METHODS**

400 **Bacterial strains, plasmids, and media**

401 *V. fischeri* and *E. coli* strains used in this study are listed in Table 1. Plasmids used in this study
402 are listed in Table 2. *V. fischeri* strains were grown at 25°C in Luria-Bertani salt (LBS) medium
403 (per liter: 25 g Difco LB broth [BD], 10 g NaCl, 50 mL 1 M Tris buffer [pH 7.5]), or TBS (per liter:
404 10 g tryptone [VWR], 20 g NaCl, 35 mM $MgSO_4$ [where noted], 10 mM calcium chloride [where
405 noted], 50 mM 1 M Tris buffer [pH 7.5]) where noted. *E. coli* strains used for cloning and
406 conjugation were grown at 37°C in Luria-Bertani (LB) medium (per liter: 25 g Difco LB broth
407 [BD]). When needed, antibiotics were added to the media at the following concentrations:
408 kanamycin, 100 µg/mL for *V. fischeri* and 50 µg/mL for *E. coli*; chloramphenicol, 1 or 5 µg/mL for
409 *V. fischeri* and 25 µg/mL for *E. coli*; erythromycin, 2.5 or 5 µg/mL for *V. fischeri*; gentamicin, 2.5
410 µg/mL for *V. fischeri* and 5 µg/mL for *E. coli*; trimethoprim, 10 µg/mL for *V. fischeri*;
411 spectinomycin, 160 µg/mL in LB for *V. fischeri*. When needed, thymidine was added at 0.3 mM
412 for *E. coli*. Growth media was solidified using 1.5% agar when needed. For Congo red agar, 40
413 µg/mL Congo red and 15 µg/mL Coomassie blue were added to LBS. For Xgal agar, 20 µg/mL
414 Xgal were added to LBS. Plasmids were introduced from *E. coli* strains into *V. fischeri* strains
415 using standard techniques (Christensen and Visick, 2020; Stabb and Ruby, 2002).
416

417 **DNA synthesis and sequencing**

418 Primers used in this study are listed in Table 3 and were synthesized by Integrated DNA
419 Technologies (Coralville, IA). Full inserts for cloned constructs and gene deletions were
420 confirmed by Sanger Sequencing at Functional Biosciences via UW-Madison. Sequence data

421 were analyzed using Benchling. PCR to amplify constructs for cloning and sequencing were
422 performed using Q5 High-Fidelity DNA polymerase (NEB), OneTaq DNA polymerase (NEB), or
423 MilliporeSigma Novagen KOD DNA Polymerase. Diagnostic PCR was performed using GoTaq
424 polymerase (Promega) or OneTaq DNA polymerase.
425
426 **Construction of multiple gene deletion mutants**
427 The multiple DGC and PDE mutants were constructed as follows. First, single gene deletions
428 were generated using PCR-SOE and *tfoX*-induced transformation methods previously described
429 (Pollack-Berti et al., 2010; Visick et al., 2018); some of these mutants have been previously
430 described (Christensen et al., 2020; Dial et al., 2021b). Briefly, regions flanking a gene of
431 interest were amplified using primers listed in Table 3 and joined to an antibiotic-resistance
432 cassette (e.g., $Trim^R/Erm^R/Spec^R$) flanked by Flp-recombinase target (FRT) sites that was
433 amplified with primers 2089 and 2090. The resulting fused PCR product was transformed into a
434 *V. fischeri* strain (generally ES114) that contained a TfoX-overproducing plasmid (pLostfoX or
435 pLostfoX-Kan plasmid (Brooks et al., 2014; Pollack-Berti et al., 2010). Selection for the
436 integrants was conducted on selective agar. The deletion/insertion was verified by PCR,
437 generally with the outside primers used to generate the flanking fragments. Next, strains with
438 multiple mutations were generated using genomic DNA from specific single mutants as follows.
439 A *tfoX*-overexpression plasmid was introduced into a mutant of interest and transformed with
440 genomic DNA containing a specific mutation, followed by selection for and verification of the
441 mutation as described above. The resulting strain carrying a *tfoX*-overexpression plasmid could
442 then serve as a recipient for the introduction of the next mutation. Because some mutants were
443 generated using the same antibiotic resistance cassette, as needed the Flp-encoding plasmid
444 pKV496 was introduced to induce the loss of the antibiotic resistance cassette and the retention
445 of a 112 bp FRT scar in the gene. Following strain construction, the integrity of each deletion
446 junction was verified with diagnostic primers listed in Table 3 to ensure that only recombination

447 at local FRT sites occurred. As noted in the strain list (Table 1), the final cassette often was left
448 in place. As an example, for Δ7PDE strain KV9601, the starting strain, KV8969 (Christensen et
449 al., 2020) (Δ*pdeV*::FRT) carrying *tfoX* plasmid pLostfoX-Kan was sequentially transformed with
450 genomic DNA carrying the Δ*VF_2480*::FRT-Erm, Δ*binA*::FRT-Trim, and Δ*VF_0087*::FRT-Spec
451 mutations. The cassettes were removed, and the *tfoX* plasmid reintroduced. Next, the
452 Δ*VF_1603*::FRT-Trim mutation was introduced, and the cassette removed. Finally, the
453 Δ*VF_A0506*::FRT-Trim mutation was introduced. Similar methods were used to generate
454 KV9599 (Δ7DGC) and the derivatives of KV9601 that carry mutations in *sypQ* or *bcsA* (the latter
455 of which was derived from strain KV8408, which carries a Tn mutation in *bcsA* (Visick et al.,
456 2018)) rather than a cassette as described above).
457
458 **Construction of *bcsA*::Tn*erm* strain**
459 Genomic DNA isolated from KV9767 (Δ6PDE *bcsA*::Tn*erm*) was introduced into MJM1100 via
460 transformation using pLostfoX-Kan (Brooks et al., 2014; Pollack-Berti et al., 2010). Mutant
461 candidates were selected using erythromycin and screened by PCR using RYI560 and RYI561
462 primers.
463
464 **Construction of the *bcsQ*'-*gfp*$^{+}$ transcriptional reporter plasmid pRYI063**
465 The *bcsQ* promoter (*bcsQ* -444 to -29; P*bcsQ*) was amplified from MJM1100 genomic DNA
466 using RYI576 and RYI577 primers that added flanking XmaI and XbaI restriction sites. The
467 amplified P*bcsQ* and pTM267 were digested with XmaI and XbaI. Digested pTM267 was treated
468 with antarctic phosphatase. Digested P*bcsQ* was ligated into digested pTM267 using T4 DNA
469 ligase (NEB). The ligation reaction was transformed into chemically competent DH5α λpir.
470 Transformant candidates were selected using chloramphenicol and confirmed by Sanger
471 sequencing using the RYI526 primer.
472

473 **Construction of the *VC1086* expression plasmid pRYI064**

474 pVSV105 was amplified using RYI578 and RYI579 primers. *VC1086*, along with 101 bp
475 upstream and 99 bp downstream, was amplified from *Vibrio cholerae* C6706 str2 genomic DNA
476 using RYI580 and RYI581 primers. *VC1086* was assembled with pVSV105 by Gibson assembly
477 using NEBuilder HiFi DNA Assembly Master Mix (NEB). The Gibson reaction was transformed
478 into chemically competent DH5α λpir and transformant candidates were selected using
479 chloramphenicol. Plasmid was screened by PCR using M13 For. (-20) and M13 Rev. (-48)
480 primers. Plasmid was confirmed by Sanger sequencing using M13 For. (-20), M13 Rev. (-48),
481 RYI584, RYI587, RYI585, and RYI586 primers.

482

483 **C-di-GMP quantification**

484 Strains were streaked on LBS agar and incubated overnight at 25°C. Liquid LBS was inoculated
485 from single colonies and grown at 25°C overnight on a rotator. 8 µL of liquid culture were
486 spotted onto LBS agar and incubated at 25°C for 24 h. Spots were resuspended in 1 mL 70%
487 Instant Ocean (IO). OD_{600}, TurboRFP (555 nm excitation/585 nm emission), and AmCyan (453
488 nm excitation/486 nm emission) for each resuspended spot were measured in triplicate using
489 BioTek Synergy Neo2 plate reader. To compare c-di-GMP levels of strains in LBS vs. IO, 1 mL
490 of overnight LBS liquid cultures were pelleted at 8000 x *g* for 10 min, resuspended in 600 µL IO,
491 and both the IO and LBS samples were incubated at room temperature for 3 hr; LBS and IO
492 strains were pelleted at 8000 x *g* for 10 min, and resuspended in 600 µL IO. OD_{600}, TurboRFP,
493 and AmCyan for each sample were measured in triplicate as described above.

494

495 **Motility assay**

496 Strains were streaked on TBS and TBS-Mg^{2+} agar and incubated overnight at 25°C. Single
497 colonies were inoculated into TBS and TBS-Mg^{2+} soft agar (0.3% agar), respectively, and

498 incubated at 25°C for 5 h. Images of plates were taken using a Nikon D810 digital camera and
499 diameter of migration was measured using ImageJ software.
500
501 **Congo red assay**
502 Strains were streaked on LBS agar and incubated overnight at 25°C. Liquid LBS was inoculated
503 with single colonies and grown at 25°C overnight on a shaker. 4 µL spots of liquid culture were
504 spotted on LBS Congo red agar and incubated 24 h at 25°C. Spots were transferred onto white
505 printer paper (Visick et al., 2018) and images were scanned as TIFF files. Congo red binding
506 was quantified using ImageJ software.
507
508 ***syp* and *bcs* expression analysis *in vitro***
509 Strains were streaked on LBS agar and incubated overnight at 25°C. Liquid media was
510 inoculated with single colonies and grown at 25°C for 24 hr on a shaker. 4 µL of overnight
511 cultures were spotted onto TBS or TBS-Ca^{2+} agar plates and grown at 25°C for 24 hr (Dial et al.,
512 2021b). Spots were imaged using the Zeiss Axio Zoom.v16 large-field 561 fluorescent stereo
513 microscope and fluorescence levels were measured using the Zen Blue Software polygon tool.
514
515 **Growth curves**
516 Strains were streaked on LBS agar and incubated overnight at 25°C. Liquid LBS was inoculated
517 with single colonies and grown at 25°C overnight on a rotator. Cultures were diluted 1:1000 in
518 LBS and grown at 25°C on a rotator to OD_{600} ~0.5. Cultures were diluted 1:100 in LBS (n = 6
519 replicates per culture) in a 96-well microtiter plate. OD_{600} was measured every 15 min for 20 hr
520 using BioTek Synergy Neo2 plate reader.
521
522 **Squid single strain colonization assay**

523 *E. scolopes* hatchlings were colonized with approximately 10^3-10^5 CFU/mL of bacteria
524 according to standard procedure (Naughton and Mandel, 2012). At 18 hpi and 48 hpi,
525 luminescence of hatchlings was measured using the Promega GloMax 20/20 luminometer and
526 euthanized by storage at -80°C. CFU counts per light organ were determined by plating
527 homogenized euthanized hatchlings and counting colonies.
528
529 **Squid competitive colonization assay**
530 Strains were grown overnight in liquid LBS at 25°C on a rotator. Strains were diluted 1:80 in
531 liquid LBS and grown to an OD_{600} of approximately 0.2. Strains were mixed in a 1:1 ratio and the
532 mixed cultures were used to inoculate *E. scolopes* hatchlings with approximately 10^3-10^4
533 CFU/mL. At 3 hpi, hatchlings were washed and transferred to 40 mL filter-sterilized Instant
534 Ocean (FSIO). Water was changed at 24 hpi and hatchlings were euthanized at 48 hpi by
535 storage at -80°C. Euthanized hatchlings were homogenized and plated on LBS-Xgal agar.
536 Competitive index of strains was measured by calculating the blue/white colony ratios as
537 previously described (Brooks et al., 2014; Naughton and Mandel, 2012).
538
539 **Squid aggregation assays**
540 Strains were grown overnight in liquid LBS at 25°C on a rotator. *E. scolopes* hatchlings were
541 inoculated with approximately 10^5-10^8 CFU/mL of bacteria. At 3 hpi, squid were anesthetized in
542 2% EtOH in FSIO and immediately dissected and imaged as described below, or were fixed in
543 4% paraformaldehyde in 1x mPBS (50 mM phosphate buffer, 0.45 M NaCl, pH 7.4) for
544 approximately 48 h. Fixed hatchlings were washed in 1x mPBS x4, dissected, and imaged using
545 the Zeiss Axio Zoom.v16 large-field 561 fluorescent stereo microscope. Aggregate area was
546 selected and fluorescence levels were measured using the Zen Blue Software polygon tool.
547 Squid with no aggregates were not included in the analyses.
548

549 **Data analysis**

550 Congo red binding was quantified using ImageJ by subtracting the WT gray value from the
551 mutant gray value and multiplying the value by -1. Fluorescence of strains in liquid culture were
552 measured using a BioTek Synergy Neo2 plate reader. Fluorescence of strains spotted on agar
553 plates and bacterial aggregates in the squid were measured using Zen Blue Software.
554 GraphPad Prism was used to generate graphs and conduct statistical analyses. Graphs were
555 further refined in Adobe Illustrator.

556

557 **ACKNOWLEDGMENTS**

558 We thank Fitnat Yildiz for providing the pFY4535 reporter plasmid,Chris Waters for input on this
559 project, and Ali Razvi and Steven Eichinger for help with strain construction. This work was
560 funded by NIGMS grant R35 GM119627 to M.J.M., NIGMS grant R35 GM130355 to K.L.V, and
561 R.Y.I. was supported from NIGMS training grant T32 GM007215.

562

563 **Table 1: Strains used in this study**

564

Strain	**Genotype**	**Source or Reference(s)**
V. fischeri		
KV4674 = ES114	Natural isolate, squid light-organ (Visick Lab Stock)	Boettcher and Ruby, 1990; Mandel et al., 2008
KV8069	KV4674 / Δ*sypQ*::FRT-Cam	Tischler et al., 2018
KV8408	KV4674 / *bcsA*::Tn*erm*	Visick et al., 2018
KV8920	KV4674 / Δ*VF_1639*::FRT-Spec	Tischler et al., 2021
KV8932	KV4674 / Δ*VF_1200*::FRT-Cam	Dial et al., 2021a
KV8969	KV4674 / Δ*pdeV*::FRT	Christensen et al., 2020
KV9599 = Δ7DGC (Low cdG)	Δ*VF_1200*::FRT Δ*mifA*::FRT Δ*VF_1245*::FRT Δ(*VF_A0342-VF_A0343*)::FRT Δ*VF_1639*::FRT Δ*mifB*::FRT-Spec	This study

Strain	Genotype	Source or Reference(s)
KV9601 = Δ6PDE (High cdG)	Δ*pdeV*::FRT Δ*VF_2480*::FRT Δ*binA*::FRT Δ*VF_0087*::FRT Δ*VF_1603*::FRT Δ*VF_A0506*::FRT-Trim	This study
KV9767	KV9601 *bcsA*::Tn*erm*	This study
KV9769	KV9601 Δ*sypQ*::FRT-Cam	This study
MJM1100 = ES114	Natural isolate, squid light-organ (Mandel Lab Stock)	Boettcher and Ruby, 1990; Mandel et al., 2008
MJM1438	MJM1100 / pM1422	Brooks and Mandel, 2016
MJM4009	MJM1100 / pFY4535	This study
MJM4135	KV9599 / pFY4535	This study
MJM4137	KV9601 / pFY4535	This study
MJM4138	KV9560 / pFY4535	This study
MJM4139	KV9569 / pFY4535	This study
MJM4140	KV9599 / pVSV102	This study
MJM4142	KV9601 / pVSV102	This study
MJM4198	KV9599 / pM1422	This study
MJM4200	KV9601 / pM1422	This study
MJM4308	KV9767 / pFY4535	This study
MJM4310	KV9769 / pFY4535	This study
MJM4312	KV9767 / pVSV102	This study
MJM4314	KV9769 / pVSV102	This study
MJM4322	KV9767 / pM1422	This study
MJM4484	MJM1100 *bcsA*::Tn*erm*	This study
MJM4592	KV9601 / pVSV103	This study
MJM4593	MJM1100 / pRYI063	This study
MJM4594	KV9599 / pRYI063	This study
MJM4595	KV9601 / pRYI063	This study
MJM4596	KV9767 / pRYI063	This study

Strain	Genotype	Source or Reference(s)
MJM4597	MJM4484 / pRYI064	This study
MJM4603	KV9601 Δ*flrA*::*erm*-bar	This study
MJM4630	MJM1100 / pRYI064	This study
MJM4631	KV9601 / pRYI064	This study
MJM4632	MJM1100 / pFY4535; pRYI064	This study
MJM4634	KV9601 / pVSV105	This study
MJM4635	MJM1100 / pFY4535; pVSV105	This study
MJM4636	KV9601 / pFY4535; pVSV105	This study
E. coli		
KV6937	DH5α / pLostfox-Kan	Brooks et al., 2014
KV8052	π3813 / pKV496	Visick et al., 2018
MJM542	DH5α λpir / pVSV102	Brennan et al., 2013a
MJM552	DH5α λpir / pVSV103	Brennan et al., 2013a
MJM579	DH5α λpir / pVSV105	Brennan et al., 2013a
MJM1422	DH5α λpir / pM1422	Brooks and Mandel, 2016
CAB1516	DH5α λpir / pVSV105	Brennan et al., 2013a
MJM3999	NEB5α / pFY4535	Zamorano-Sánchez et al., 2019
MJM4580	DH5α λpir / pRYI063	This study
MJM4625	DH5α λpir / pRYI064	This study

565
566
567 **Table 2: Plasmids used in this study**
568

Plasmid	Description	Source or Reference(s)
pEVS104	Conjugal helper plasmid (Kan^R)	Stabb and Ruby, 2002
pFY4535	c-di-GMP reporter plasmid ($Gent^R$)	Zamorano-Sánchez et al., 2019
pJJC4	Vector carrying *tfoX* and *litR* genes (Cam^R)	Cohen et al., 2021

pKV494	Vector carrying FRT-Erm^R	Visick et al., 2018
pKV495	Vector carrying FRT-Cam^R	Visick et al., 2018
pKV496	pLostfoX-Kan backbone containing the FLP recombinase (Kan^R)	Visick et al., 2018
pKV521	Vector carrying FRT-Spec^R	Visick et al., 2018
pLostfoX-Kan	TfoX induction vector for chitin-pathway transformation (Kan^R)	Brooks et al., 2014
pM1422	pTM267 *sypA'-gfp*$^+$ (Cam^R)	Brooks and Mandel, 2016
pMCL2	Vector carrying FRT-Trim^R	Visick et al., 2018
pRYI063	pTM267 *bcsQ'-gfp*$^+$ (Cam^R)	This study
pRYI064	pVSV105 carrying *VC1086* (Cam^R)	This study
pVSV102	Constitutive GFP (Kan^R)	Dunn et al., 2006
pVSV103	Constitutive LacZ (Kan^R)	Dunn et al., 2006
pVSV105	Complementation vector (Cam^R)	Brennan et al., 2013a

569
570
571 **Table 3: Primer List**
572

Primer Name	Sequence (5'-3')	Notes
2089	CCATACTTAGTGCGGCCGCCTA	Forward primer to amplify antibiotic resistance cassette
2090	CCATGGCCTTCTAGGCCTATCC	Reverse cassette to amplify antibiotic resistance cassettes
2537	AGTGCCTCATATAAGGGTTAAG	Outside forward PCR primer for the Δ(*VF_A0342-A0343*) construct
2538	taggcggccgcactaagtatggTGTTACGTCAACAA CCTTTTGG	Inside reverse PCR primer for the Δ(*VF_A0342-A0343*) construct
2543	ggataggcctagaaggccatggATGGCGGATACTG CATTGTATC	Inside forward PCR primer for the Δ(*VF_A0342-A0343*) construct
2544	CCAAATCGACAGAGATCCCC	Outside reverse PCR primer for the Δ(*VF_A0342-A0343*) construct
2593	GCCAATGCAGATATGACAAAGG	Outside forward PCR primer for the Δ*VF_1245* construct
2558	taggcggccgcactaagtatggTAAGCGCTGAAGA CGAGATTG	Inside reverse PCR primer for the Δ*VF_1245* construct
2559	ggataggcctagaaggccatggATTGAACAAGCAG ATAAGGCGC	Inside forward PCR primer for the Δ*VF_1245* construct

2560	GCATTCATTAGTGATGTGCGTG	Outside reverse PCR primer for the Δ*VF_1245* construct
2905	ggataggcctagaaggccatggCACTTCGTGTTAAAGAATTTATAC	Confirmation of Δ*VF_1639*
2564	CTAACCATTCATGCAAGAACC	Confirmation of Δ*VF_1639*
2577	TAAAGCAGCAGCTGAGCAAG	Confirmation of Δ*VF_1200*
2580	GTTTGGTGAGTACCAATCGC	Confirmation of Δ*VF_1200*
2585	CAAAGCATCAAAAACTCACTTGC	Outside forward PCR primer for the Δ*VF_0087* construct
2586	taggcggccgcactaagtatggAATGCTTTGAACACTAAATGAGAG	Inside reverse PCR primer for the Δ*VF_0087* construct
2587	ggataggcctagaaggccatggGGTGAGCCTAAATCGTTACAC	Inside forward PCR primer for the Δ*VF_0087* construct
2588	AACGAACGCCACAAACTCAC	Outside reverse PCR primer for the Δ*VF_0087* construct
944	CGCATACGTTTCTACCGTTTC	Confirmation of ΔVF_0087
945	CCAAGCTGAACGAAGTGGAC	Confirmation of ΔVF_0087
2598	CACTGATGGTTTAGAGCTTGG	Outside forward PCR primer for the Δ*mifA* construct
2599	taggcggccgcactaagtatggCAGCTCTGTTTGATATAGTGTCC	Inside reverse PCR primer for the Δ*mifA* construct
2600	ggataggcctagaaggccatggAGTGAAATGGATCAAATCGCATG	Inside forward PCR primer for the Δ*mifA* construct
2601	TTGATGCGAGATTGAAATACGC	Outside reverse PCR primer for the Δ*mifA* construct
2618	AGAGCAGCTCGTGAGTTATC	Confirmation of Δ*pdeV*
2621	CTTCCATAGTAAGAACCTCTGC	Confirmation of Δ*pdeV*
2648	GCATGTGTACCAAGTAAGCTTG	Outside forward PCR primer for the Δ*VF_A0506* construct
2649	taggcggccgcactaagtatggCATTGTCCATTCATAAGATGGGC	Inside reverse PCR primer for the Δ*VF_A0506* construct
2650	ggataggcctagaaggccatggCGAGGTCAACAATTTGACCC	Inside forward PCR primer for the Δ*VF_A0506* construct
2651	GGCATTGATGAGTCTTAAGCTG	Outside reverse PCR primer for the Δ*VF_A0506* construct
2674	CTAAAGTGCACAAACCATGGC	Outside forward PCR primer for the Δ*VF_1603* construct
2675	taggcggccgcactaagtatggGTCTAAGATTGGTTGACGAGC	Inside reverse PCR primer for the Δ*VF_1603* construct

2676	ggataggcctagaaggccatggTCTGCCAAATGGGTAGATGAG	Inside forward PCR primer for the Δ*VF_1603* construct
2677	TTATTGCAGGTGCTGCACTG	Outside reverse PCR primer for the Δ*VF_1603* construct
2678	TTGGCCACGGTGATCGAAAG	Outside forward PCR primer for the Δ*VF_2480* construct
2679	taggcggccgcactaagtatggTATCGGTTGTCTGGCAACG	Inside reverse PCR primer for the Δ*VF_2480* construct
2680	ggataggcctagaaggccatggACCTACCAAGAAGCGGTTAAG	Inside forward PCR primer for the Δ*VF_2480* construct
2681	TTGCTGCTAATCGTGACAGC	Outside reverse PCR primer for the Δ*VF_2480* construct
1152	CAGTAGAGTCACTACCGTTG	Outside forward PCR primer for the Δ*binA* construct
2714	taggcggccgcactaagtatggTTGTTCAGGAATGTCGATGGC	Inside reverse PCR primer for the Δ*binA* construct
2715	ggataggcctagaaggccatggCACTTTGTGTAATGGGCACTC	Inside forward PCR primer for the Δ*binA* construct, inside forward
2716	GCCTCTGGATTTGGATAGTG	Outside reverse PCR primer for the Δ*binA* construct
850	gggcccAGAATAAACTGCTACTATCT	Confirmation of Δ*binA*
445	AAAACAGTAATCAGGGTGGAACG	Confirmation of Δ*binA*
2753	ATAGATGGTAAAGCGTCATACC	Outside forward PCR primer for the Δ*mifB* construct
2754	taggcggccgcactaagtatggACGTAAGCTCACATATGGGC	Inside reverse PCR primer for the Δ*mifB* construct
2755	ggataggcctagaaggccatggTTTACCGTTGCTGATGAACATATG	Inside forward PCR primer for the Δ*mifB* construct
2756	CAAACCATTGAACGCCATGATC	Outside reverse PCR primer for the Δ*mifB* construct
M13 For. (-20)	GTAAAACGACGGCCAGT	For amplification of gene inserts in pVSV105
M13 Rev. (-48)	AGCGGATAACAATTTCACACAGG	For amplification of gene inserts in pVSV105
RYI526	GTGCCCATTAACATCACCATCTAATTCA	Primer to confirm replacement of Kan^R cassette with promoter of choice
RYI560	GATATCAATGAGGTAATGCTTTTATTTTTTGCGAA	Forward primer to confirm transposon insertion in *bcsA*
RYI561	GCATAATTCTTACTTGGTTGCATGGTTTG	Reverse primer to confirm transposon insertion in *bcsA*
RYI576	gctaCCCGGGggtttgtggcatgacgatcact	Forward primer to amplify P*bcsQ* with XmaI restriction site

RYI577	cacgTCTAGAactaactttattctccaatgtattaactacac attttgg	Reverse primer to amplify P*bcsQ* with XbaI restriction site
RYI578	CAGGTCGACTCTAGAGGATCCCC	Forward primer to linearize pVSV105 for Gibson assembly
RYI579	CAGGCATGCAAGCTTGAGTATTCTAT	Reverse primer to linearize pVSV105 for Gibson assembly
RYI580	tactcaagcttgcatgcctgGAAGAACACCATGGCA AAATAAAGCTC	Forward primer to amplify *VC1086* with 101 bp upstream for Gibson assembly with pVSV105
RYI581	gatcctctagagtcgacctgCGGTTAAGCGCTTTCA AAATATCGTTTTC	Reverse primer to amplify *VC1086* with 99 bp downstream for Gibson assembly with pVSV105
RYI584	GGTGATAGAGATTAATCGCCGCTATCC	Sequencing primer for *VC_1086*
RYI585	GATAGCTTTCAGAACCCAGCACCT	Sequencing primer for *VC_1086*
RYI586	GTTACTGAGCGTCGCGGAGG	Sequencing primer for *VC_1086*
RYI587	TTATGGAGATAGTTTGTTATGGAGATAGTT CAGGA	Sequencing primer for *VC_1086*

573

574 **REFERENCES**

575 Bassis CM, Visick KL. 2010. The cyclic-di-GMP phosphodiesterase BinA negatively regulates
576 cellulose-containing biofilms in *Vibrio fischeri*. *J Bacteriol* **192**:1269–1278.
577 Bennett BD, Essock-Burns T, Ruby EG. 2020. HbtR, a Heterofunctional Homolog of the
578 Virulence Regulator TcpP, Facilitates the Transition between Symbiotic and Planktonic
579 Lifestyles in *Vibrio fischeri*. *MBio* **11**:2020.03.31.019356.
580 Boettcher KJ, Ruby EG. 1990. Depressed light emission by symbiotic *Vibrio fischeri* of the
581 sepiolid squid *Euprymna scolopes*. *J Bacteriol* **172**:3701–3706.
582 Brennan CA, DeLoney-Marino CR, Mandel MJ. 2013a. Chemoreceptor VfcA mediates amino
583 acid chemotaxis in *Vibrio fischeri*. *Appl Environ Microbiol* **79**:1889–1896.
584 Brennan CA, Mandel MJ, Gyllborg MC, Thomasgard KA, Ruby EG. 2013b. Genetic
585 determinants of swimming motility in the squid light-organ symbiont *Vibrio fischeri*.
586 *Microbiologyopen* **2**:576–594.
587 Brooks JF 2nd, Gyllborg MC, Cronin DC, Quillin SJ, Mallama CA, Foxall R, Whistler C,
588 Goodman AL, Mandel MJ. 2014. Global discovery of colonization determinants in the squid
589 symbiont *Vibrio fischeri*. *Proc Natl Acad Sci U S A* **111**:17284–17289.
590 Brooks JF 2nd, Mandel MJ. 2016. The histidine kinase BinK Is a negative regulator of biofilm
591 formation and squid colonization. *J Bacteriol* **198**:2596–2607.
592 Burgos HL, Burgos EF, Steinberger AJ, Suen G, Mandel MJ. 2020. Multiplexed competition in a
593 synthetic squid light organ microbiome using barcode-tagged gene deletions. *mSystems*
594 **5**:e00846–20.
595 Christensen DG, Marsden AE, Hodge-Hanson K, Essock-Burns T, Visick KL. 2020. LapG
596 mediates biofilm dispersal in *Vibrio fischeri* by controlling maintenance of the VCBS-
597 containing adhesin LapV. *Mol Microbiol* **114**:742–761.
598 Christensen DG, Visick KL. 2020. *Vibrio fischeri*: Laboratory Cultivation, Storage, and Common
599 Phenotypic Assays. *Curr Protoc Microbiol* **57**:e103.
600 Cohen JJ, Eichinger SJ, Witte DA, Cook CJ, Fidopiastis PM, Tepavčević J, Visick KL. 2021.
601 Control of competence in *Vibrio fischeri*. *Appl Environ Microbiol* **87**.
602 doi:10.1128/AEM.01962-20
603 Colvin KM, Irie Y, Tart CS, Urbano R, Whitney JC, Ryder C, Howell PL, Wozniak DJ, Parsek
604 MR. 2012. The Pel and Psl polysaccharides provide *Pseudomonas aeruginosa* structural
605 redundancy within the biofilm matrix. *Environ Microbiol* **14**:1913–1928.
606 Dial CN, Eichinger SJ, Foxall R, Corcoran CJ, Tischler AH, Bolz RM, Whistler CA, Visick KL.
607 2021a. Quorum Sensing and Cyclic di-GMP Exert Control Over Motility of *Vibrio fischeri*
608 KB2B1. *Front Microbiol* **12**:690459.
609 Dial CN, Speare L, Sharpe GC, Gifford SM, Septer AN, Visick KL. 2021b. Para-Aminobenzoic
610 Acid, Calcium, and c-di-GMP Induce Formation of Cohesive, Syp-Polysaccharide-
611 Dependent Biofilms in *Vibrio fischeri*. *MBio* e0203421.
612 Dunn AK, Millikan DS, Adin DM, Bose JL, Stabb EV. 2006. New rfp- and pES213-derived tools
613 for analyzing symbiotic *Vibrio fischeri* reveal patterns of infection and *lux* expression *in situ*.
614 *Appl Environ Microbiol* **72**:802–810.
615 Graf J, Dunlap PV, Ruby EG. 1994. Effect of transposon-induced motility mutations on
616 colonization of the host light organ by *Vibrio fischeri*. *J Bacteriol* **176**:6986–6991.
617 Hall CL, Lee VT. 2018. Cyclic-di-GMP regulation of virulence in bacterial pathogens. *Wiley*
618 *Interdiscip Rev RNA* **9**. doi:10.1002/wrna.1454
619 Hayes CA, Dalia TN, Dalia AB. 2017. Systematic genetic dissection of PTS in *Vibrio cholerae*
620 uncovers a novel glucose transporter and a limited role for PTS during infection of a
621 mammalian host. *Mol Microbiol* **104**:568–579.
622 Heindl JE, Wang Y, Heckel BC, Mohari B, Feirer N, Fuqua C. 2014. Mechanisms and regulation
623 of surface interactions and biofilm formation in *Agrobacterium*. *Front Plant Sci* **5**.

624 doi:10.3389/fpls.2014.00176
625 Hengge R, Gründling A, Jenal U, Ryan R, Yildiz F. 2016. Bacterial signal transduction by cyclic
626 Di-GMP and other nucleotide second messengers. *J Bacteriol* **198**:15–26.
627 Jones BW, Nishiguchi MK. 2004. Counterillumination in the Hawaiian bobtail squid, *Euprymna*
628 *scolopes* Berry (Mollusca: Cephalopoda). *Mar Biol* **144**:1151–1155.
629 Koehler S, Gaedeke R, Thompson C, Bongrand C, Visick KL, Ruby E, McFall-Ngai M. 2019.
630 The model squid-vibrio symbiosis provides a window into the impact of strain- and species-
631 level differences during the initial stages of symbiont engagement. *Environ Microbiol*
632 **21**:3269–3283.
633 Ludvik DA, Bultman KM, Mandel MJ. 2021. Hybrid histidine kinase BinK represses *Vibrio*
634 *fischeri* biofilm signaling at multiple developmental stages. *J Bacteriol* **203**:e0015521.
635 Mandel MJ, Schaefer AL, Brennan CA, Heath-Heckman EAC, Deloney-Marino CR, McFall-Ngai
636 MJ, Ruby EG. 2012. Squid-derived chitin oligosaccharides are a chemotactic signal during
637 colonization by *Vibrio fischeri*. *Appl Environ Microbiol* **78**:4620–4626.
638 Mandel MJ, Stabb EV, Ruby EG. 2008. Comparative genomics-based investigation of
639 resequencing targets in *Vibrio fischeri*: focus on point miscalls and artefactual expansions.
640 *BMC Genomics* **9**:138.
641 McFall-Ngai MJ, Ruby EG. 1991. Symbiont recognition and subsequent morphogenesis as early
642 events in an animal-bacterial mutualism. *Science* **254**:1491–1494.
643 Millikan DS, Ruby EG. 2003. FlrA, a σ^{54}-Dependent Transcriptional Activator in *Vibrio fischeri*, Is
644 Required for Motility and Symbiotic Light-Organ Colonization. *J Bacteriol* **185**:3547–3557.
645 Millikan DS, Ruby EG. 2002. Alterations in Vibrio fischeri motility correlate with a delay in
646 symbiosis initiation and are associated with additional symbiotic colonization defects. *Appl*
647 *Environ Microbiol* **68**:2519–2528.
648 Morris AR, Darnell CL, Visick KL. 2011. Inactivation of a novel response regulator is necessary
649 for biofilm formation and host colonization by *Vibrio fischeri*. *Mol Microbiol* **82**:114–130.
650 Naughton LM, Mandel MJ. 2012. Colonization of *Euprymna scolopes* squid by *Vibrio fischeri*. *J*
651 *Vis Exp* e3758.
652 Nawroth JC, Guo H, Koch E, Heath-Heckman EAC, Hermanson JC, Ruby EG, Dabiri JO, Kanso
653 E, McFall-Ngai M. 2017. Motile cilia create fluid-mechanical microhabitats for the active
654 recruitment of the host microbiome. *Proc Natl Acad Sci U S A* **114**:9510–9516.
655 Nikolakakis K, Monfils K, Moriano-Gutierrez S, Brennan CA, Ruby EG. 2015. Characterization
656 of the *Vibrio fischeri* Fatty Acid Chemoreceptors, VfcB and VfcB2. *Appl Environ Microbiol*
657 **82**:696–704.
658 Nyholm SV, Stabb EV, Ruby EG, McFall-Ngai MJ. 2000. Establishment of an animal-bacterial
659 association: recruiting symbiotic vibrios from the environment. *Proc Natl Acad Sci U S A*
660 **97**:10231–10235.
661 O'Shea TM, Deloney-Marino CR, Shibata S, Aizawa S-I, Wolfe AJ, Visick KL. 2005. Magnesium
662 promotes flagellation of *Vibrio fischeri*. *J Bacteriol* **187**:2058–2065.
663 O'Shea TM, Klein AH, Geszvain K, Wolfe AJ, Visick KL. 2006. Diguanylate cyclases control
664 magnesium-dependent motility of *Vibrio fischeri*. *J Bacteriol* **188**:8196–8205.
665 Pollack-Berti A, Wollenberg MS, Ruby EG. 2010. Natural transformation of *Vibrio fischeri*
666 requires *tfoX* and *tfoY*. *Environ Microbiol* **12**:2302–2311.
667 Robinson CD, Sweeney EG, Ngo J, Ma E, Perkins A, Smith TJ, Fernandez NL, Waters CM,
668 Remington SJ, Bohannan BJM, Guillemin K. 2021. Host-emitted amino acid cues regulate
669 bacterial chemokinesis to enhance colonization. *Cell Host Microbe* **29**:1221–1234.e8.
670 Römling U, Galperin MY, Gomelsky M. 2013. Cyclic di-GMP: the first 25 years of a universal
671 bacterial second messenger. *Microbiol Mol Biol Rev* **77**:1–52.
672 Rotman ER, Bultman KM, Brooks JF 2nd, Gyllborg MC, Burgos HL, Wollenberg MS, Mandel
673 MJ. 2019. Natural strain variation reveals diverse biofilm regulation in squid-colonizing
674 *Vibrio fischeri*. *J Bacteriol* **201**:e00033–19.

675 Ruby EG, Asato LM. 1993. Growth and flagellation of *Vibrio fischeri* during initiation of the
676 sepiolid squid light organ symbiosis. *Arch Microbiol* **159**:160–167.
677 Spurbeck RR, Tarrien RJ, Mobley HLT. 2012. Enzymatically active and inactive
678 phosphodiesterases and diguanylate cyclases are involved in regulation of motility or
679 sessility in *Escherichia coli* CFT073. *MBio* **3**. doi:10.1128/mBio.00307-12
680 Stabb EV, Ruby EG. 2002. RP4-based plasmids for conjugation between *Escherichia coli* and
681 members of the Vibrionaceae. *Methods Enzymol* **358**:413–426.
682 Sycuro LK, Ruby EG, McFall-Ngai M. 2006. Confocal microscopy of the light organ crypts in
683 juvenile *Euprymna scolopes* reveals their morphological complexity and dynamic function in
684 symbiosis. *J Morphol* **267**:555–568.
685 Tamayo R, Schild S, Pratt JT, Camilli A. 2008. Role of cyclic Di-GMP during El Tor biotype
686 *Vibrio cholerae* infection: characterization of the *in vivo*-induced cyclic Di-GMP
687 phosphodiesterase CdpA. *Infect Immun* **76**:1617–1627.
688 Thompson CM, Tischler AH, Tarnowski DA, Mandel MJ, Visick KL. 2019. Nitric oxide inhibits
689 biofilm formation by *Vibrio fischeri* via the nitric oxide sensor HnoX. *Mol Microbiol* **111**:187–
690 203.
691 Tischler AH, Vanek ME, Peterson N, Visick KL. 2021. Calcium-Responsive Diguanylate Cyclase
692 CasA Drives Cellulose-Dependent Biofilm Formation and Inhibits Motility in *Vibrio fischeri*.
693 *MBio* **12**:e0257321.
694 Visick KL. 2009. An intricate network of regulators controls biofilm formation and colonization by
695 *Vibrio fischeri*. *Mol Microbiol* **74**:782–789.
696 Visick KL, Hodge-Hanson KM, Tischler AH, Bennett AK, Mastrodomenico V. 2018. Tools for
697 rapid genetic engineering of *Vibrio fischeri*. *Appl Environ Microbiol* **84**:e00850–18.
698 Waters CM, Lu W, Rabinowitz JD, Bassler BL. 2008. Quorum sensing controls biofilm formation
699 in Vibrio cholerae through modulation of cyclic di-GMP levels and repression of *vpsT*. *J*
700 *Bacteriol* **190**:2527–2536.
701 Wolfe AJ, Visick KL. 2010. Roles of diguanylate cyclases and phosphodiesterases in motility
702 and biofilm formation in *Vibrio fischeri* In: Wolfe AJ, Visick KL, editors. The Second
703 Messenger Cyclic Di-GMP. Washington, DC: American Society for Microbiology Press. pp.
704 186–200.
705 Yip ES, Geszvain K, DeLoney-Marino CR, Visick KL. 2006. The symbiosis regulator RscS
706 controls the *syp* gene locus, biofilm formation and symbiotic aggregation by *Vibrio fischeri*.
707 *Mol Microbiol* **62**:1586–1600.
708 Yip ES, Grublesky BT, Hussa EA, Visick KL. 2005. A novel, conserved cluster of genes
709 promotes symbiotic colonization and σ^{54}-dependent biofilm formation by *Vibrio fischeri*. *Mol*
710 *Microbiol* **57**:1485–1498.
711 Zamorano-Sánchez D, Xian W, Lee CK, Salinas M, Thongsomboon W, Cegelski L, Wong GCL,
712 Yildiz FH. 2019. Functional Specialization in *Vibrio cholerae* Diguanylate Cyclases: Distinct
713 Modes of Motility Suppression and c-di-GMP Production. *MBio* **10**.
714 doi:10.1128/mBio.00670-19